J Nanostruct 13(4): 1184-1194, Autumn 2023

RESEARCH PAPER

Enhanced Thermoplasmonic Effect in Core/Multi Shell Hybrid Nanostructures

*Nada Abbas Mohammed, A. K. Kodeary *, Wajeha Abdl Daim*

Department of Laser Physics, College of Science, University of Babylon, Babylon, Iraq

ARTICLE INFO

Article History:
Received 02 June 2023
Accepted 25 September 2023
Published 01 October 2023

Keywords:
Core/multi-shell nanoparticle
Hybrid nanostructures
Photothermal effect
Thermoplasmonic

ABSTRACT

We present an experimental study of the photothermal properties of core/multi-shell hybrid nanostructures prepared by laser ablation. The hybrid multi-shell nanostructures consist of gold-silver and silver-gold sandwich with silicon shell in between. The results show that the plasmonic properties can be are tune by controlling the structure of the core/shell nanoparticles. The optical absorption was measured using a UV–V is spectrophotometer for the samples, and the intensity and position of the plasmon were monitored depending on the dielectric properties of the samples. The thermoplasmonic properties are studied by monitoring the local temperature increase of the samples when the samples are heated by lasers of different wavelengths. The results show that not only an extreme tunability in the surface plasmon resonances can be obtained but also considerable enhanced photothermal effects in terms of temperature rise. Furthermore, the temperature rise depends on the laser effect. This result opens the possibility of using the core/multi-shell NPs as efficient heat sources in many applications.

How to cite this article
Mohammed N., Kodeary A., Abdl Daim W. Enhanced Thermoplasmonic Effect in Core/Multi Shell Hybrid Nanostructures . J Nanostruct, 2023; 13(4):1184-1194. DOI: 10.22052/JNS.2023.04.026

INTRODUCTION

Over the last decade, there have been an increasing interest by researchers in use of plasmonic nanomaterials as effective sources of heat remotely controlled by light named as thermoplasmonics. Thermoplasmonic is a field of study involving the light-triggered local temperature rise of plasmonic materials (also called “photothermal” heating) [1]. Plasmonic nanoparticles play a substantial role in this field of research of thermoplasmonics due to their optical, electronic, thermal, and catalytic properties and also have aroused keen interest due to the distinguished feature of surface plasmon resonance (SPR), which is characterized by plasmonic metal nanoparticles only [2]. The SPR is a collective oscillation of conduction electrons possessed by metal nanoparticles, which is excited by an electromagnetic field at special wavelengths [3].

This field has been widely exploited for a large number of applications, including biomedical sensors [4,5], photothermal imaging [6], drug delivery [7], cancer thermotherapy [8,9], disinfection and sterilization [10].

Despite considerable progress in the techniques of synthesis of nanomaterials and their use in several fields, especially the medical field, a great deal remains to be understood about the fundamentals of thermoplasmonic nanomaterials,

* *Corresponding Author Email: ahmed.kodeary88@uobabylon.edu.iq*

in particular the physiological and biological mechanisms they trigger. Plasmonic nanoparticles are used for their high capacity to boost a local temperature based on optical heating and also with optical nearfield enhancement and hot-carrier injection [11].

Thermoplasmonics represents a significant research area with pivotal, economic, and societal impact that could contribute to the development of the medical nanofield. In particular, hot-electron injection involves plasmonic metal electrons by laser, and it has the ability to raise the temperature which could not happen otherwise through conventional heating [12].

Therefore, with the use of plasmonic nanoparticles (NPs) as effective light absorbers, this approach provides key features compared with conventional heating. One of these features is that the heating laser provides reduced spatial scale to enable heating over a micrometric area.

This allows the heat to not spread to the surrounding areas. Also, the plasmonic heating may produce a high temperature rise with moderate lighting. Pulsed and continuous laser light brings the nanoparticles to a superheated state. Moreover, the advantage of plasmonic NPs, when sized down to a few nanometres, they can also feature effective catalytic activity [12].

Furthermore, previous research into thermoplasmonic effects has primarily focused on bare noble metals such as Au and Ag NPs in a variety of morphologies such as spherical, ellipsoids, rods, disks, rings, and stars, among others [13-18].

Since the absorption by the bare noble metal leads to the dissipation of light into resistive thermal energy, optically excited noble metal/semiconductor core/shell NPs can thereby be exploited as efficient heat sources in a set of applications instead of the bare noble metal in the field of thermoplasmonics [3]. Therefore, core/shell nanoparticles are good candidates for this application [19].

The core/shell plasmonic nanoparticles have a highly geometrically tunable optical resonance. This in turn gives controllability of the refractive index and the dielectric properties of the nanomaterial [3].

The concentric incorporation of either a spherical gold or silver nanocore into the silicone nanoshell, followed by the plasmonic coating layer as the next nanoshell, leads to different plasmonic behaviors and optimized photothermal properties of the nanostructure. There has been a lot of experimental work on metal/silica NPs in various applications, but there is still a need to discover the tunable photothermal properties of the core/shell nanostructures and the role of the shell in the photothermal response, which deserves more attention.

Their plasmonic properties for core/shell NPs are mostly linked to the interaction between the size of the core and the thickness of the shell. The plasmonic coupling strength can be determined by the core size and the shell thickness. Whilst, the plasmon coupling strength makes them efficient

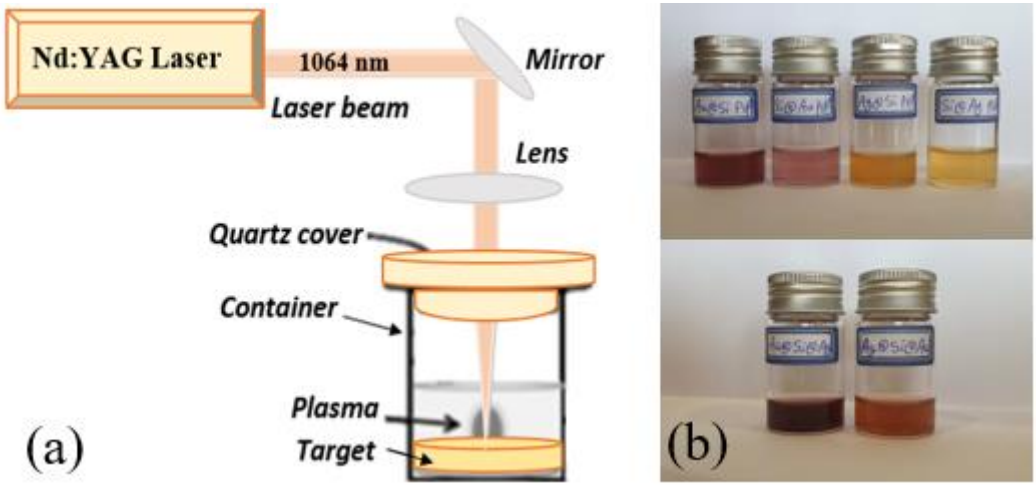

Fig. 1. a- Diagram of the experimental configuration used to prepare NPs by laser ablation confined in a liquid medium, b- the colloidal solution preparations samples.

for light-to-heat conversion by using metal/silicon core/shell nanoplasmonics when the wavelength shift plasmon band is in the IR-region. Thus, the development of IR-region plasmonic materials still has many challenges [20].

Our recent studies have reported enhanced properties of thermoplasmonic for the core/multi-shell hybrid nanostructures. They have the ability to be used for photothermal in biomedical applications as an effective anti-bacterial. In such a hybrid system, Au/Si/Ag have characteristic plasmon absorption from the UV to NIR spectral region, whereas noble bare metals have narrow wavelength plasmonic absorption. This allows the use of lasers of different wavelengths to irritate the thermoplasmonic. This study will provide useful information about the thermoplasmonic properties of core/shell nanoparticles based on metalic/silicone and the optimal use of the plasmonic nanoparticles for thermoplasmonic bio-medical applications based on heating.

MATERIALS AND METHODS

In this work, we have prepared Ag, Au, and Si bare nanoparticles and also prepared core/shell NPs as well as core/multi-shell NPs based on Au/Si/Ag by laser ablation. The experiments were conducted by using the 1064 nm Nd: YAG laser have 5 ns pulse width, and 6 Hz repetition rate. Energy per pulse was 120 mJ focused directly on the sample placed in a liquid medium. Fig. 1 shows the schematic diagram of the experimental setup of laser ablation in liquid mediums.

The laser pulses were directed at the pure (99.9%) (Au and Ag) metal targets with a thickness of 2 mm, and also the Si target with a thickness of 2 mm, were used as targets, immersed in an aqueous solution of the Polyvinylpyrrolidone (PVP) polymer. A mixture of 1 % PVP was dissolved in deionized water with a magnetic stirrer to obtain a more stable solution in the vessel, a glass container with a high reflectivity mirror and a lens with focal length 150mm. The height of water over the target was maintained at 10mm. In the meantime, the entire system slowly rotates about its vertical axis during the ablation process to prevent developing deep holes in the target, and therefore keep the same surface conditions for each laser pulse. Subsequently, the distance between the target and the lens has been set to get the focus point on the target.

A two-stage sequential ablation method was used for the preparation of bimetallic core/shell NPs. First, a core NPs colloid solution was prepared using laser ablation of an Au target in deionized water with PVP polymer. Irradiation of the target endured for 3 min and has been accompanied by a homogeneous liquid coloration in a characteristic bright red color due to the SPR band of Au NPs in the visible region, followed by ablation of the Si target in a colloidal solution Au NPs freshly prepared. The Si NPs act as a shell and form a core for ablated hot Au species. However, the ablation duration was 1–3 minutes for Si to obtain core/shell morphology with variable shell thickness.

For the purpose of preparing a core/multi-shell NP, a step is added to the above series, followed by the ablation of the Ag target in a pre-prepared

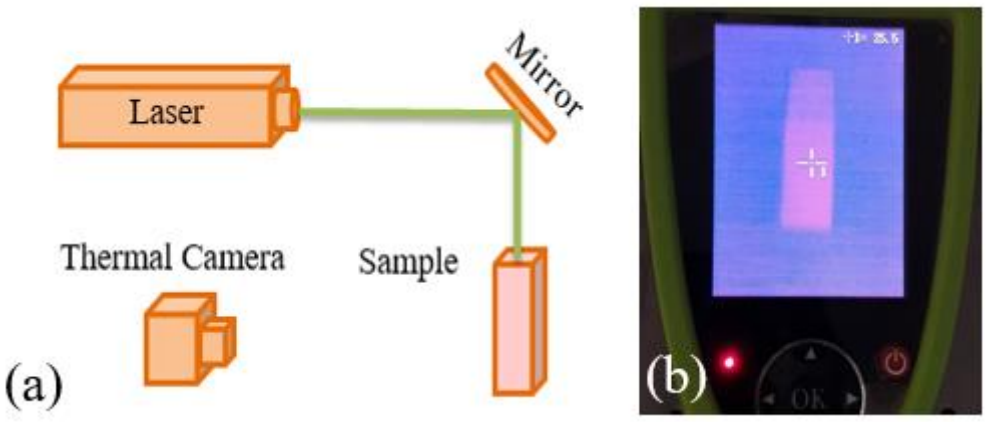

Fig. 2. a- Diagram of the experimental setup used of the thermoplasmonic imaging, b- the thermal images at room temperature recorded by thermal camera for the colloidal solution preparations samples.

colloidal solution. The Ag NPs act as a second shell for the Au/Si core/shell NPs to produce a three-layer system (core/multi-shell NPs). After preparation, every the solutions were stirred at RT into an ultrasonic tub for about 5 min. A similar procedure was performed using Ag as a core with Si as a first shell to produce Ag@Si core/shell NPs, and the same procedure was used for Au as a second shell to produce Ag@Si@Au core/multi-shell NPs. The colors of the colloidal suspensions as in Fig. 1b obtained in our samples are the characteristic ones due to the presence of Ag, and Au NPs. Namely, this is proof that the sample has a SPR absorption spectrum that changes thusly as per their NP sizes.

At the end of the experiments, we obtained eleven samples of PVP mixtures for the purpose of comparing them. We have three samples of bare nanoparticles (Au,Ag, and Si NPs). We also have six samples of core/shell NPs (Au@Si, Ag@Si, Si@Au, Si@Ag, Au@Ag, and Ag@Au NPs), as well as two samples of core/multi-shell NPs (Au@Si@Ag, and Ag@Si@Au NPs).

Moreover, to determine the photothermal effect for all samples used in this work. We measure the temperature elevation of a colloidal by the absorbing NPs by the heat rise record with the NPs behaving act as efficient point sources of heat. In general, a key issue examined here is the convertibility of light into the heat of the core/shell plasmonic NPs of different nanostructures [21]. It has used the high resolution thermal imaging camera (type of EIRC5s) during laser direct irradiation in order to reveal the temperature elevation, which is caused by the conversion of light into heat with the help of plasmonic nanostructures. Three lasers were used to illuminate the prepared samples. First, we used CW Nd: YAG laser, operates with 30 mW power and 532 nm wavelength. Second, we used

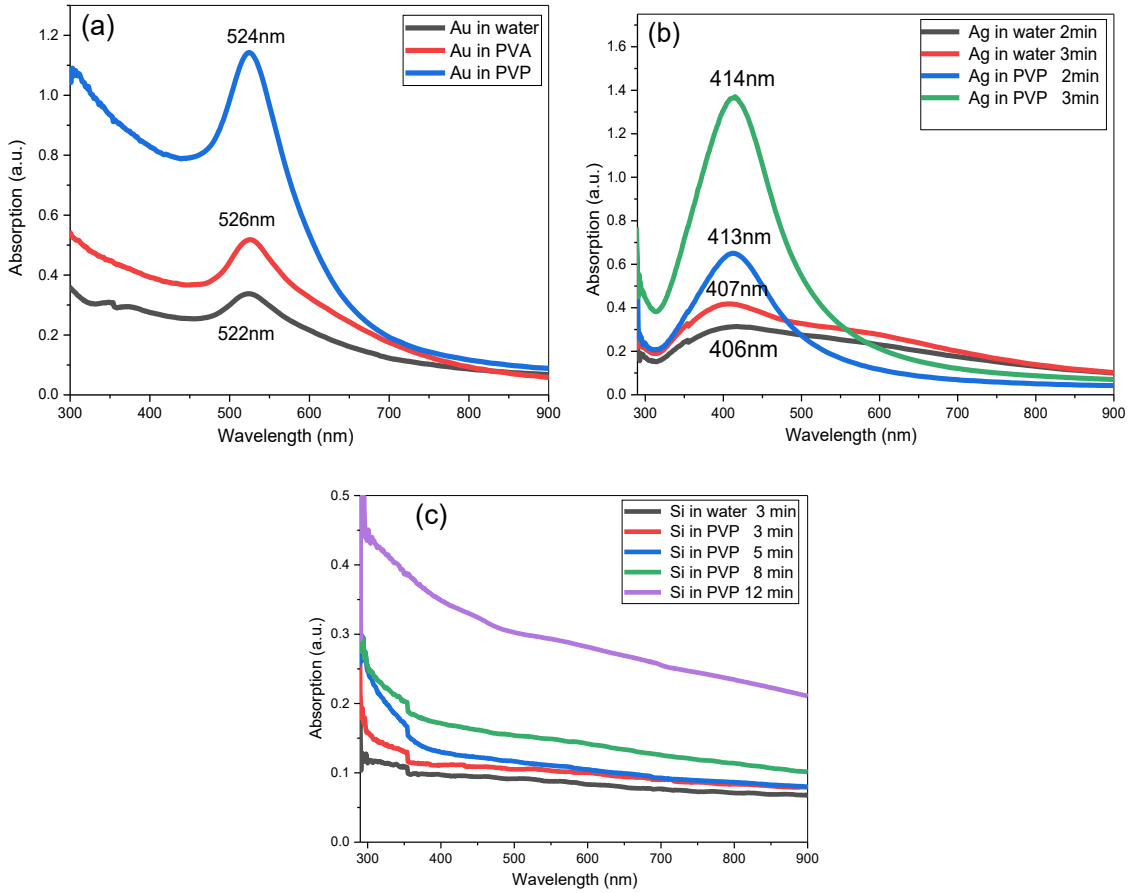

Fig. 3. Absorption spectra of the bare NPs; a- gold NPs in different liquid medias, b- Silver NPs for different ablation time, and c- Silicon NPs for different ablation time.

a 30 mW diode laser with a wavelength (473 nm). Subsequently, we used a 30 mW diode laser with a wavelength (405 nm) to compare and study the effects of the laser wavelength on the samples, duration of the luminance time was 2 minutes for all lasers, with the setup as shown in Fig. 2.

RESULTS AND DISCUSSION

The optical spectra for freshly prepared samples by the laser ablation method in liquid media by the peak absorption of the samples were measured using a UV–Vis spectrophotometer (wavelength range of 190–900 nm) model (CECIL7200). The behavior is shown in Fig. 3 of the bare nanoparticles.

Fig. 3a shows the UV-Vis absorption of the gold NPs in different liquid media. The liquid media used were distilled deionized water, PVP polymer (Polyvinyl pyrrolidone) dissolved in 1% deionized distilled water using a magnetic stirrer. For comparison, we used 1% PVA polymer (Polyvinyl alcohol) dissolved in deionized distilled water by a magnetic stirrer at room temperature, in order to obtain more stability for the colloidal solution. The absorbance spectra of the gold nanoparticles were recorded for all the solutions used in this research, and it is noted from Fig. 3a that each sample has an absorbance peak due to surface plasmon resonance (SPR) for the gold NPs, it is an absorbance spectrum according to nanoparticle sizes and structures, with peak absorbance SPR is more pronounced in PVP solution due to the increased stability of the medium [22], compared to other solutions, which makes it more stable than aqueous medium and PVA polymer.

Moreover, due to larger NPs in PVP medium, which was confirmed by FE-SEM in Fig. 4, we have red shift in SPR wavelength from 522 to 526 nm. This fact leads to increasing the refractive index of the medium leads to the ability to modify the SPR wavelength of the samples. It is noticed from Fig. 3b that the absorption spectrum of silver NPs increased in PVP polymer compared to distilled water at different ablation times for the same reason. Increasing the size of NPs in turn leads to increasing the refractive index of the medium. We also notice a shift towards long wavelengths (red shift) for the absorption spectrum of about (406-414nm), when changing both the liquid medium and the ablation time, which is evidence of an increase in the size and stability of NPs in the PVP polymer matrix compared to deionized water.

The absorption spectrum of the silicon NPs samples in deionized water solution and the PVP solution for different ablation times is illustrated in Fig. 3c. These figures indicate that each sample has an absorption intensity, which can see more effective absorption of silicone in the PVP matrix due to the increased stability of the medium and increase the intensity of silicon absorption with increasing ablation time.

The results showed that the average size of gold NPs in the PVP polymeric solution increases when compared to the deionized distilled water solution (from 15 nm to 20 nm) as in Fig. 4, and this is due to the reason for NPs to be collected inside the polymer. This result agrees with [23,24].

We also noticed that the density of gold NPs

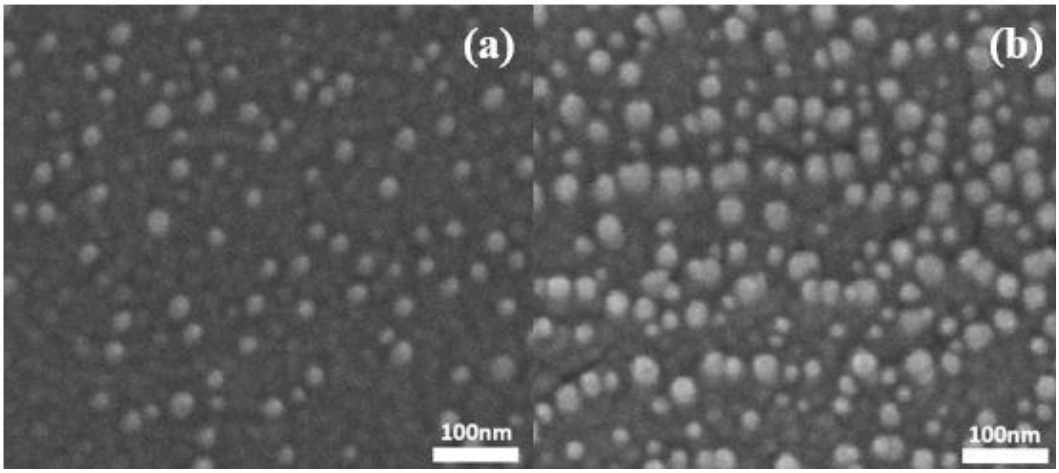

Fig. 4. Image of FESEM for a- Au NPs in water, and b- Au NPs in PVP.

in the PVP polymeric solution is greater when compared to the distilled water, and this is due to the fact that the polymeric solution is more stable to keep the nanoparticles from sedimentation to the bottom of the container after a period of time.

As it was expected, in the spectra of absorption for the metallic/metallic core/shell NPs and the metallic/semiconductor/metallic core/multi-shell NPs samples, we can be clearly see two distinct peaks which come from the absorption of plasmonic noble metals (gold and silver) in the nanostructure, as shown in Fig. 5b. But we clearly notice that when adding silicon to the core/shell NPs samples, there is an increase in the intensity of absorption with a redshift in the wavelength when compared to the bare NPs, as shown in Fig. 5a. We have tunability and a red shift in the SPR wavelength, which is confirmed in these hybrid nanostructures samples as shown in Table 1.

Silicon shell over the metal core leads to the extended near-field due to coupling between the nanocore of the noble metal and the nanoshell of the silicon, which also changes the position SPR towards the far wavelength (redshifts) accompanied by a decrease of the maximum near-field enhancement. Subsequently, increasing the total size of core/shell NPs makes near-field enhancement weaken at their redshifted resonance [20-26].

In addition, we use a Field Emission Scanning Electron Microscopy (FE-SEM) model (JSM-7610F) to determine and evaluate the morphology of the samples (size and shape nanoparticles). The samples were obtained of metal phase/semiconductor core/shell nanostructures in quasi-spherical morphology. We can notice that all the examined samples successfully formed the shell clearly and distinctly. The behavior is shown in Fig. 6.

The core/shell nanostructures are made of gold, silver, and silicon particles in an aqueous solution of a PVP polymer, with the core size ranging from 20–30 nm and the shell from 10–20 nm for Au@Si NPs as in Fig. 6a, and Si@Ag NPs as in Fig. 6b, with a slight increase in the average size of samples for the core/multi-shell hybrid nanostructures, as in

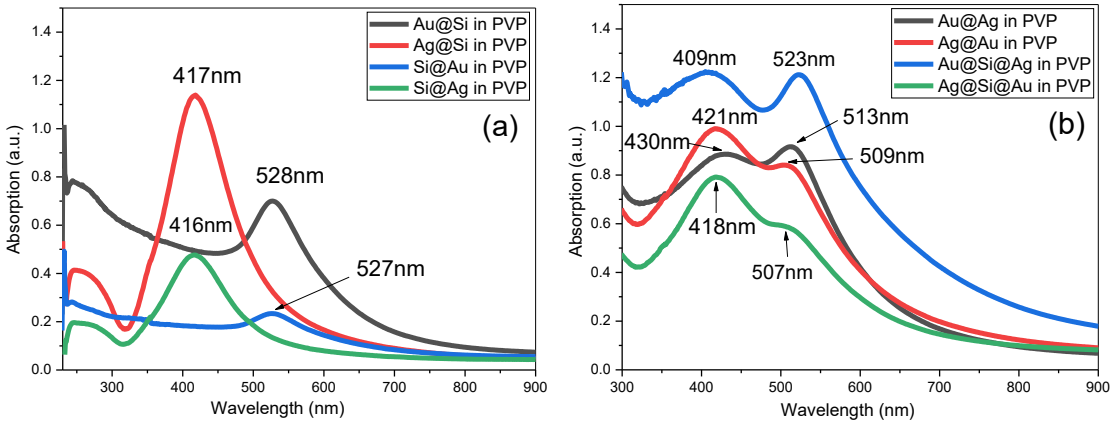

Fig. 5. Absorption spectra of the core/shell NPs; a- metallic/semiconductor core/shell NPs for different compositions, b- metallic/metallic core/shell NPs and metallic/semiconductor/metallic core/multi-shell NPs for different compositions.

Table 1. the SPR controlling with different compositions of hybrid NPs.

Samples	SPR in PVP matrix
Au@Si NPs	528 nm
Ag@Si NPs	417 nm
Si@Au NPs	527 nm
Si@Ag NPs	416 nm
Au@Ag NPs	513@430 nm
Ag@Au NPs	421@509 nm
Au@Si@Ag NPs	523@409 nm
Ag@Si@Au NPs	418@507 nm

Fig. 6c and Fig. 6d.

We know that the dielectric properties of material are very important and have a major role in

determining the intensity and position of the peak of SPR of the plasmonic NPs [23].

As expected, the coupling between the plasmonic noble metals with semiconductors yields a change in the dielectric properties. This in turn leads to a change the real and imaginary part of the refractive index for all samples [24,27].

Through the relationships between the real and imaginary dielectric coefficients, the refractive index of the samples can be calculated, $\varepsilon_1 = n^2 - k^2$ and $\varepsilon_2 = 2nk$ [23,24].

The behavior is shown in Fig. 7, which shows the real dielectric parameters of the core/shell NPs, and Fig. 8, which shows the imaginary dielectric parameters of the used core/shell NPs. The real and imaginary parts of the dielectric coefficient in these figures were extracted from the empirically measured absorption spectra to find the main optical properties of the samples in the PVP polymer matrix.

Moreover, the coupling between silicon NPs and plasmonic metal NPs in core/shell NPs leads to a high tunability of the surface plasmon position. As well as a clear increase in the real dielectric constant, and thus increasing the real refractive index, it is understood when we compare Fig. 7a for core/shell NPs with Fig. 7b for core/multi-shell NPs, as two distinct peaks are observed in both the imaginary and the real parts of the refractive indexes.

It is clear that the SPR was improved for the Au@Si@Ag NPs sample, where the silver in the envelope region increases the plasmonic property, resulting in a clear redshift in wavelength. By

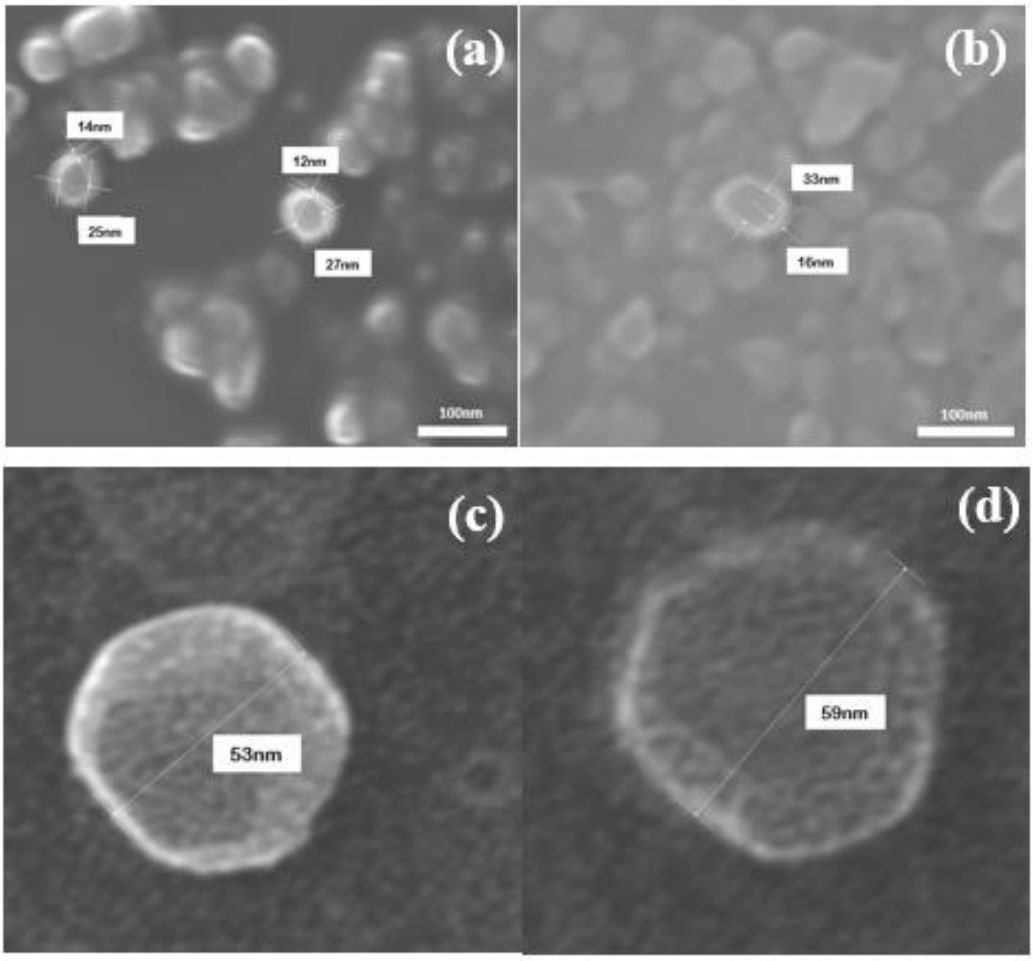

Fig. 6. FESEM image of a- Au@Si NPs, b- Si@Ag NPs, c- Au@Si@Ag NPs, and d- Ag@Si@Au NPs in PVP.

contrast, in the Ag@Si@Au NPs sample, no significant change in the position and amount of the SPR was observed.

To better understand our results, we discuss the imaginary dielectric properties as a function of the imaginary refractive index, as it gives a clearer picture of the surface plasmon behavior of nanoparticles, just as we studied the real value of the refractive index, where one complements the other. This change can be realized by the fact that the properties of the plasmon intensity and position can be determined with high accuracy by describing the imaginary dielectric properties of the material through the imaginary refractive index. When silicon nanoshell of core/shell NPs samples becomes an improvement in plasmon intensity, as in Fig. 8a. We also notice an increase in the plasmon intensity of the Au@Si@Ag NPs in the imaginary dielectric constant curve, as in Fig. 8b. This is because of an increase in the refractive index, as well as the coupling between the plasmonic properties of nano-gold and nano-silver with the semiconductor properties of nano-silicone, which led to a change in the refractive index of all samples. Our results are consistent with studies [22-25].

According to the above results, the enhancement in the properties, wavelength shift, and tunability in position SPR is very important for the study of the thermoplasmonic properties of the samples. The thermal behavior of metallic nanoparticles are defined by their ability to absorb light and convert it into heat. The heat generation depends on the shape and size of NPs, as well as

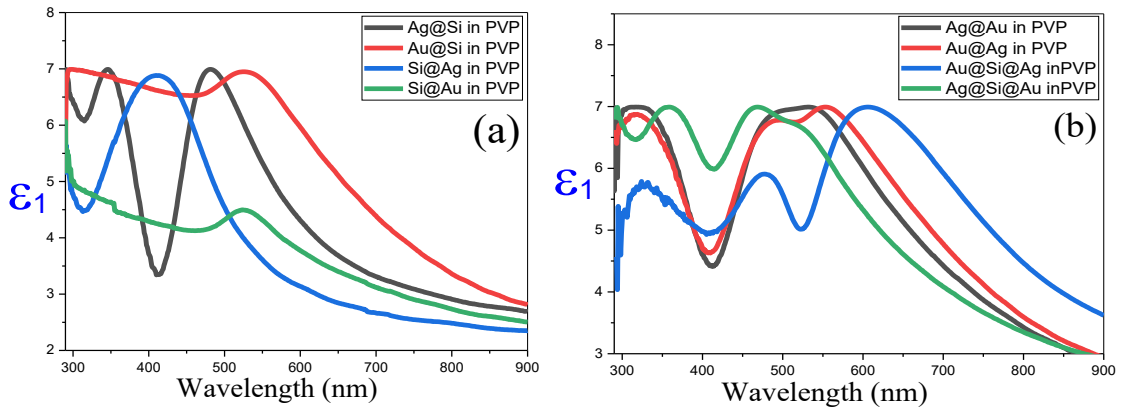

Fig. 7. the real dielectric coefficient as a function of wavelength in the matrix of PVP polymers, for samples (a) metal/ semiconductor core/shell NPs, (b) metal/metal and metal/ semiconductor/metal core/shell NPs.

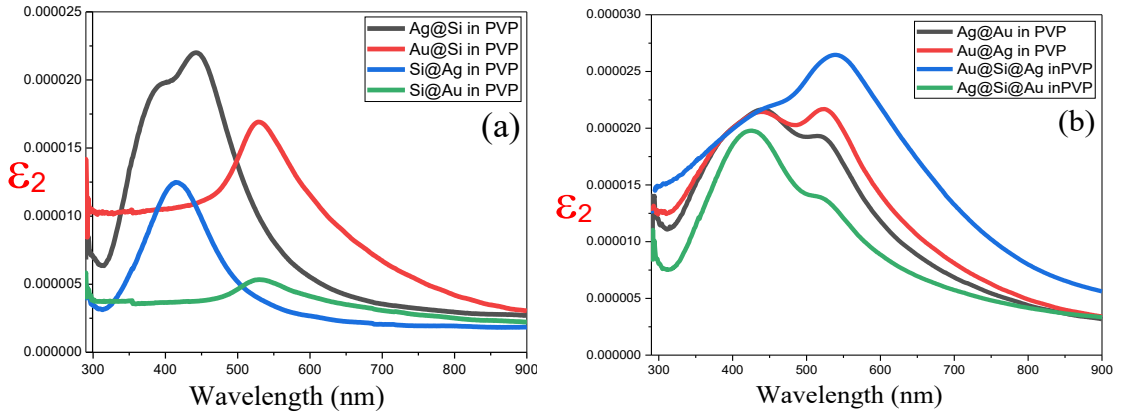

Fig. 8.the imaginary dielectric coefficient as a function of wavelength in the matrix of PVP polymers, for samples (a) metal/ semiconductor core/shell NPs, (b) metal/metal and metal/ semiconductor/metal core/shell NPs.

the number of NPs in the sample and also the type of material. As increasing the number of NPs in the sample improves its thermal response to light.

We monitor the temperature at the nanoscale for all samples irradiated by laser, using a high-resolution thermal camera from the experimental point of view at room temperature. We are looking for a new opportunity in the thermoplasmonics field by exploiting the different applications for nanomaterial technology in advanced biomedical applications. Besides, from the thermal camera images, we can clearly see the cell position has a temperature higher than the surrounding medium, as in Fig. 2b. It is evident from this result, the nanomaterials used in this work, which have the ability to absorb light and generate thermoplasmonic and heat up the surrounding medium under laser lighting. This result is very similar to ref [28].

Furthermore, the thermoplasmonic technique is mainly primarily based of the photothermal effect induced by a focused laser beam that remotely generates a confined temperature field at the desired position with high controllability among the laser parameters, such as the wavelength of laser, intensity, pulse width, and illumination time. With the possibility of changing these parameters to achieve the desired thermal effect [28,29]. The phenomenon of nanoparticles absorption is usually associated with the scattering phenomenon of laser radiation, leading to light attenuation and re-diffusion (spatial redistribution) of the laser beam energy [28,29].

Experimentally, show our results that the sample of the Au@Si@Ag core/multi-shell NPs that temperature rises by ΔT = 7.4 °C, 7.1 °C, and 6.9 °C under laser lighting the 20 mW 405nm, 473nm, and 532nm respectively. Correspondingly, the sample of the Ag@Si@Au core/multi-shell NPs sample heat up by ΔT = 6.3 °C, 6.6 °C, and 8.2 °C, under the influence of the same lasers above (see Fig. 9).

As seen from Fig. 9 core/multi-shell nanoparticles have a higher temperature than the core/shell nanoparticles, and this in turn has a higher temperature than bare NPs. Besides, the results show that core/shell NPs samples produce more heat than individual bare NPs samples, due to the redistribution of an electron/hole pair in the metal/semiconductor interfaces that leads to the height of the Schottky barrier in core/shell samples [23,30].

Moreover, it can be clearly observed from Fig. 9 that Au@Si@Ag NPs have a higher temperature than the Ag@Si@Au NPs, when illuminated by green laser, due to the fact that the SPR peak is close to the wavelength of the laser (532 nm) used for the samples excitation.

Our findings demonstrated that a temperature elevation was encouraging for the use of core/

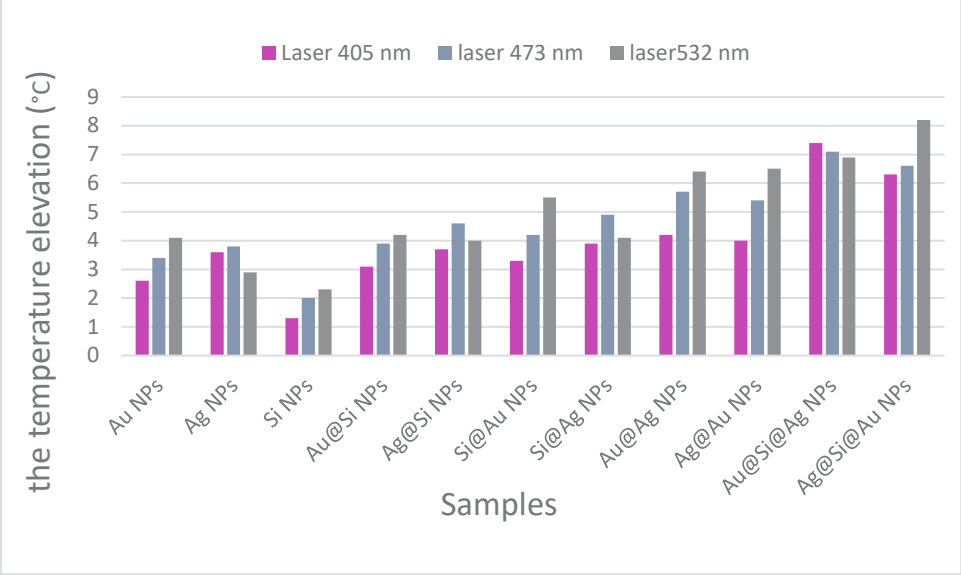

Fig, 9. Experimental heat generation by 20 mW CW laser (405,473, and 532 nm) illumination of all samples in this study.

multi-shell NPs samples for thermoplasmonic applications in living tissues, despite the fact, so various previous studies pronounced that a temperature elevation in living tissues required a range over 3–13 °C [28]. As a result, the core/multi-shell NPs proposed in this study have the potential to be used in cancer treatment and other biomedical applications.

CONCLUSION

In summary, we have synthesized plasmonic metallic nanoparticles (NPs) of Au NPs, and Ag NPs. We also used Si NPs as a partner for noble metals for the production of hybrid nanoparticles as core/shell NPs and core/multi-shell NPs. The nanostructures are dispersed in aqueous solution of PVP polymer and prepared by pulsed laser ablation. The study includes characterizing the thermoplasmonic properties of the nanostructures by using CW lasers at wavelengths 405 nm, 473 nm, and 532 nm. Our results show significant adjustability of the position and intensity of the SPR for each set of NPs that is can be useful in many optical device designs. In addition, the results show that the core/shell NPs and the core/multi-shell NPs have the ability of exhibiting extremely agile tunability in the position of the SPR, and considerably enhanced thermoplasmonic effect is comparison with the bare metal NPs. The temperature elevation of Ag@Si@Au NPs was higher than Au@Si@Ag NPs under 532 nm laser illumination, due to the higher absorption of the Ag@Si@Au at the excitation wavelength in comparison with the Au@Si@Ag structure. Due to the same reason, Au@Si@Ag shows the maximum heating at 405 nm excitation over the other structures. This study proved that the core/multi-shell hybrid nanostructures could be used as a nanoheat sources in many applications including biomedical applications.

CONFLICT OF INTEREST

The authors declare that there is no conflict of interests regarding the publication of this manuscript.

REFERENCES

1. Kim M, Lee J-H, Nam J-M. Plasmonic Photothermal Nanoparticles for Biomedical Applications. Advanced science (Weinheim, Baden-Wurttemberg, Germany). 2019;6(17):1900471-1900471.
2. Dai H, Ding R, Li M, Li Y, Yang G, Song D, et al. Abnormal thermal effects on the surface plasmon resonance of Ag nanoparticles on the surface of silicon. Thin Solid Films. 2015;584:378-381.
3. Li Q, Zhang W, Zhao D, Qiu M. Photothermal Enhancement in Core-Shell Structured Plasmonic Nanoparticles. Plasmonics. 2014;9(3):623-630.
4. Unser S, Bruzas I, He J, Sagle L. Localized Surface Plasmon Resonance Biosensing: Current Challenges and Approaches. Sensors (Basel, Switzerland). 2015;15(7):15684-15716.
5. Anker JN, Hall WP, Lyandres O, Shah NC, Zhao J, Van Duyne RP. Biosensing with plasmonic nanosensors. Nature Materials. 2008;7(6):442-453.
6. Wang Y, Barhoumi A, Tong R, Wang W, Ji T, Deng X, et al. $BaTiO_3$-core Au-shell nanoparticles for photothermal therapy and bimodal imaging. Acta Biomater. 2018;72:287-294.
7. Bohara RA. Introduction and Types of Hybrid Nanostructures for Medical Applications. Hybrid Nanostructures for Cancer Theranostics: Elsevier; 2019. p. 1-16.
8. Ricciardi L, Sancey L, Palermo G, Termine R, De Luca A, Szerb EI, et al. Plasmon-mediated cancer phototherapy: the combined effect of thermal and photodynamic processes. Nanoscale. 2017;9(48):19279-19289.
9. De Sio L, Placido T, Comparelli R, Lucia Curri M, Striccoli M, Tabiryan N, et al. Next-generation thermo-plasmonic technologies and plasmonic nanoparticles in optoelectronics. Progress in Quantum Electronics. 2015;41:23-70.
10. Baffou G, Cichos F, Quidant R. Applications and challenges of thermoplasmonics. Nature Materials. 2020;19(9):946-958.
11. Ghobadi TGU, Ghobadi A, Ozbay E, Karadas F. Strategies for Plasmonic Hot-Electron-Driven Photoelectrochemical Water Splitting. ChemPhotoChem. 2018;2(3):161-182.
12. Baffou G. Thermoplasmonics: Cambridge University Press; 2017 2017/10/19.
13. Choi KW, Kim DY, Ye SJ, Park OO. Shape- and size-controlled synthesis of noble metal nanoparticles. Adv Mater Res. 2014;3(4):199-216.
14. Zhang Y, Huang R, Zhu X, Wang L, Wu C. Synthesis, properties, and optical applications of noble metal nanoparticle-biomolecule conjugates. Chin Sci Bull. 2012;57(2-3):238-246.
15. Geonmonond RS, Silva AGMD, Camargo PHC. Controlled synthesis of noble metal nanomaterials: motivation, principles, and opportunities in nanocatalysis. An Acad Bras Cienc. 2018;90(1 suppl 1):719-744.
16. Yang Z, Han X, Lee HK, Phan-Quang GC, Koh CSL, Lay CL, et al. Shape-dependent thermo-plasmonic effect of nanoporous gold at the nanoscale for ultrasensitive heat-mediated remote actuation. Nanoscale. 2018;10(34):16005-16012.
17. Tan SF. Real-Time Imaging of Au–Ag Core-Shell Nanoparticles Formation. Springer Theses: Springer Singapore; 2018. p. 97-112.
18. Ghosh Chaudhuri R, Paria S. Core/Shell Nanoparticles: Classes, Properties, Synthesis Mechanisms, Characterization, and Applications. Chem Rev. 2011;112(4):2373-2433.
19. Amendola V, Pilot R, Frasconi M, Maragò OM, Iatì MA. Surface plasmon resonance in gold nanoparticles: a review. J Phys: Condens Matter. 2017;29(20):203002.
20. Wang H, Li M. Near-Infrared II Thermoplasmonics of Cuprous Selenide Multilayer Nanoshells: The Role of the Plasmonic Core. The Journal of Physical Chemistry Letters. 2021;12(20):4928-4935.

21. Norton SJ, Vo-Dinh T. Photothermal effects of plasmonic metal nanoparticles in a fluid. J Appl Phys. 2016;119(8).
22. Gatea, et al. Thermoplasmonic of Single Au@SiO_2 and SiO_2@Au Core Shell Nanoparticles in Deionized Water and Poly-vinylpyrrolidoneMatrix. Baghdad Science Journal. 2019;16(2):0376.
23. Kodeary AK, Hamidi SM. Tunable Piezophotonic Effect on Core-Shell Nanoparticles Prepared by Laser Ablation in Liquids under External Voltage. Journal of Nanotechnology. 2019;2019:1-11.
24. Kodeary AK, Hamidi SM, Moradlou R. Voltage controlled properties of piezo-magneto-plasmonic core/shell nanoparticles. Nano-Structures and Nano-Objects. 2020;21:100415.
25. Al-Ibraheemi S, Al-Ibraheemi FA, Gatea MA. Nonlinear Optical Properties of Gold-silica Nano-particles. 2019 2nd International Conference on Engineering Technology and its Applications (IICETA); 2019/08: IEEE; 2019. p. 25-30.
26. Mbarak H, Kodeary AK, Hamidi SM, Mohajarani E, Zaatar Y. Control of nonlinear refractive index of AuNPs doped with nematic liquid crystal under external electric field. Optik. 2019;198:163299.
27. Majhi SM, Rai P, Yu Y-T. Facile Approach to Synthesize Au@ZnO Core–Shell Nanoparticles and Their Application for Highly Sensitive and Selective Gas Sensors. ACS Applied Materials and Interfaces. 2015;7(18):9462-9468.
28. Kodeary AK, Gatea MA, Haddawi SF, Hamidi SM. Tunable thermo-piezo-plasmonic effect on core/shell nanoparticles under laser irradiation and external electric field. Optical and Quantum Electronics. 2020;52(2).
29. Rashidi-Huyeh M, Palpant B. Thermal response of nanocomposite materials under pulsed laser excitation. J Appl Phys. 2004;96(8):4475-4482.
30. Chen F, Wu W-B, Li S-Y, Klein A. Energy band alignment at ferroelectric/electrode interface determined by photoelectron spectroscopy. Chinese Physics B. 2014;23(1):017702.